THE JOURNAL OF PHYSICAL CHEMISTRY C

Article

Characterization of Planar Lead Halide Perovskite Solar Cells by Impedance Spectroscopy, Open Circuit Photovoltage Decay and Intensity-Modulated Photovoltage/Photocurrent Spectroscopy

Adam Pockett, Giles E. Eperon, Timo Peltola, Henry J. Snaith, Alison B. Walker, Laurence M Peter, and Petra J. Cameron

J. Phys. Chem. C, **Just Accepted Manuscript** • Publication Date (Web): 21 Jan 2015

Characterization of Planar Lead Halide Perovskite Solar Cells by Impedance Spectroscopy, Open Circuit Photovoltage Decay and Intensity-Modulated Photovoltage/Photocurrent Spectroscopy

Adam Pockett[1], Giles E. Eperon[2], Timo Peltola[3], Henry J. Snaith[2], Alison Walker[3], Laurence M. Peter*[1], and Petra J. Cameron*[1]

1. Department of Chemistry, University of Bath, Bath BA2 7AY, United Kingdom

2. Clarendon Laboratory, Parks Road, Oxford, OX1 3PU, United Kingdom

3. Department of Physics, University of Bath, Bath BA2 7AY, United Kingdom

KEYWORDS. Impedance, intensity-modulated, non-ideality factor, open circuit voltage decay, perovskite, recombination.

ABSTRACT: Thin film lead halide perovskite cells, where the perovskite layer is deposited directly onto a flat titania blocking layer, have reached AM 1.5 efficiencies of over 15%,[1] showing that the mesoporous scaffold used in early types of perovskite solar cells is not essential. We have used a variety of techniques to gain a better understanding of thin film perovskite cells prepared by a solution-based method. Twelve cells were studied, which showed AM 1.5 efficiencies of ≈ 11%. The properties of the cells were investigated using impedance spectroscopy, intensity modulated photovoltage spectroscopy (IMVS), intensity modulated photocurrent spectroscopy (IMPS) and open circuit photovoltage decay (OCVD). Despite the fact that all 12 cells were prepared at the same time under nominally identical conditions, their behavior fell into two distinct groups. Half the cells exhibited ideality factors of m≈2.5 and the other half showed ideality factors of m≈5. Impedance spectroscopy carried out under illumination at open circuit for a range of intensities showed that the cell capacitance was dominated by the geometric capacitance of the perovskite layer rather than the chemical or diffusion capacitance due to photogenerated carriers. The voltage dependence of the recombination resistance gave ideality factors similar to those derived from the intensity dependence of the open circuit voltage. The IMVS time constant was determined by the product of the geometric capacitance and the recombination resistance. The two types of cell gave very different OCVD responses. The cells with m≈2.5 showed a persistent photovoltage effect that was absent in the case of the cells with higher ideality factors. The IMPS responses provide evidence of minor efficiency losses by recombination under short circuit conditions.

Introduction

The rapid development of organometal halide perovskite solar cells[2-5] based on $CH_3NH_3PbI_3$ and its analogs continues to set new records in terms of efficiency[6] that already far exceed those for dye-sensitized solar cells or organic photovoltaics. The high open circuit voltages and high external quantum efficiencies point to unusually slow recombination of electrons and holes in the perovskite absorber layer, with second order rate constants for uncontacted thin films reported to be four orders lower than the Langevin limit for bimolecular recombination.[7] The reasons for such slow recombination are currently a central topic of discussion,[8-10] and it has been suggested that the formation of ferroelectric domains may lead to spatial separation of electrons and holes[11-12]. It has also been reported that the lead halide perovskites exhibit a photoinduced giant dielectric effect (GDE) with a relaxation time constant in the region of seconds.[13] The high open circuit voltages (in excess of 1 V) also indicate that the built-in voltage of the junction must be unusually high (> 1 V) relative to the band gap of the perovskite (ca. 1.5 eV). Reported band alignments in the TiO_2|perovskite|spiro-OMeTAD structure[14] suggest that the built-in voltage in the thin perovskite layer could exceed 1.2V.

In principle, electron-hole recombination can occur either in the bulk of the perovskite or at the contacts, which are made using materials that are selective for extraction of electrons (e.g. TiO_2) or of holes (e.g. spiro-OMeTAD). A number of methods have been used to study electron-hole recombination including transient microwave[9, 15-16] and terahertz[9, 16-17] measurements, photoluminescence,[18] transient absorbance,[7, 18] EBIC,[19] photo-

voltage and photocurrent transients,[20] impedance[21-24] and open circuit voltage decay.[25] Many of these studies have characterized the properties of perovskite cells fabricated using mesoporous oxide substrates of either TiO_2 or Al_2O_3. However, interest is increasingly being focused on planar junction perovskite cells that appear in many instances to operate as p-i-n devices.[19] For this reason we chose to characterize batches of planar perovskite cells using a range of complementary techniques, namely impedance, intensity modulated photovoltage spectroscopy (IMVS), intensity modulated photocurrent spectroscopy (IMPS), open circuit photovoltage decay (OCPVD) and steady-state photovoltage measurements as a function of light intensity. The use of these six techniques on a large number of cells allowed us to assess the consistency of the conclusions.

The series of 12 planar perovskite devices could be divided clearly into two groups on the basis of the intensity dependences of the open circuit voltage, which corresponded to diode ideality factors that clustered either around ~2.5 or around ~5.0. The high frequency impedance and intensity-modulated photovoltage (IMVS) responses of the cells were modelled satisfactorily using a simple lumped RC circuit. At low frequencies an additional feature was observed which Juárez-Pérez et al.[13] have attributed to a photo-induced giant dielectric effect. The influence of the GDE on the low frequency impedance response has been modelled by Bisquert et al.[26], but in this paper the low frequency feature has not been included in modelling. Substantial information about the cell was extracted using the simple lumped model at mid and high frequencies, and we are currently measuring and modelling the low frequency feature separately. The results obtained at open circuit by impedance and IMVS are in good agreement, both indicating that for open circuit voltages below 0.9 V, the geometric capacitance associated with charge in the contacting phases (TiO2 and spiro-OMeTAD) is larger than the chemical (or diffusion) capacitance associated with the build-up of electrons and holes in the perovskite absorber, even at the highest light intensities used here (equivalent to 0. 1 sun). The voltage dependence of the recombination resistance gave non-ideality factors close to those derived from the intensity dependence of the open circuit voltage. OCVD also reveals that some cells exhibit a persistent photovoltage that extends the decay time into the region of seconds when the voltage falls below 0.4V.

Experimental

Perovskite precursor preparation: Methylamine iodide (MAI) was prepared by reacting methylamine, 33 wt% in ethanol (Sigma-Aldrich), with hydroiodic acid (HI),57 wt% in water (Sigma-Aldrich), at room temperature. HI was added dropwise while stirring. Upon drying at 100°C, a white powder was formed, which was washed with ethanol and dried overnight in a vacuum oven before use.

To form the non-stoichiometric $CH_3NH_3PbI_{3-x}Cl_x$ precursor solution, methylammonium iodide and lead (II) chloride (98%, Sigma-Aldrich) are dissolved in anhydrous *N,N*-Dimethylformamide (DMF) at a 3:1 molar ratio of MAI to $PbCl_2$, with final concentrations 0.88M lead chloride and 2.64M methylammonium iodide. This solution is stored under a dry nitrogen atmosphere.

Substrate preparation: Devices were fabricated on fluorine-doped tin oxide (FTO) coated glass (Pilkington, 7Ω $\square^{-1}$). To prevent shunting upon contact with measurement pins, FTO was removed from regions under the anode contact by etching with 2M HCl and zinc powder. Substrates were then cleaned sequentially in 2% Hellmanex detergent, acetone, propan-2-ol and oxygen plasma. A hole-blocking layer of compact TiO_2 was deposited by spin-coating a mildly acidic solution of titanium isopropoxide in anhydrous ethanol (350µl in 5ml ethanol with 0.013M HCl), and annealed at 500°C for 30 minutes. Spin-coating was carried out at 2000rpm for 60 seconds.

Perovskite solar cell fabrication: A total of 12 cells was fabricated in groups of 3 cells on one substrate, each with a pixel area of 0.15 cm^2. To form the perovskite layer, the non-stoichiometric precursor was spin-coated on the substrate in a nitrogen-filled glovebox at 2000rpm for 45 seconds. After spin-coating, the films were left to dry at room temperature in the glovebox for 30 minutes, to allow slow solvent evaporation. They were then annealed on a hotplate in the glovebox at 90°C for 180 minutes and subsequently at 120°C for 15 minutes.

A hole-transporting layer was then deposited via spin-coating a 0.79M solution of 2,2',7,7'-tetrakis-(N,N-di-p-methoxyphenylamine)9,9'-spirobifluorene (spiro-OMeTAD) in chlorobenzene, with additives of lithium bis(trifluoromethanesulfonyl)imide (0.0184M) and 4-tert-butylpyridine (0.0659M). Spin-coating was carried out at 2000rpm for 45 seconds. Devices were then left overnight in air for the spiro-OMeTAD to dope via oxidation. Finally, gold electrodes were thermally evaporated under vacuum of ~10^{-6} Torr, at a rate of ~0.1 nm s^{-1}, to complete the devices.

Solar cell characterization: The current density–voltage (J-V) curves were measured (2400 Series SourceMeter, Keithley Instruments) under simulated AM 1.5 sunlight at 100 $mWcm^{-2}$ irradiance generated by an Abet Class AAB sun 2000 simulator, with the intensity calibrated with an NREL calibrated KG5-filtered Si reference cell. The mismatch factor was calculated to be 1.2% between 400 and 1100nm. The solar cells were masked with a metal aperture to define the active area, typically 0.0625cm^{-2} and measured in a light-tight sample holder to minimize any edge effects.

The cells were stored in a nitrogen glove box between measurements to minimize degradation. Open circuit voltages were measured as a function of light intensity using a 625 nm light emitting diode (LED) (Thorlabs MRLED). The incident photon flux was controlled using neutral density filters (Edmund Optics) and measured using a calibrated silicon photodiode (Newport 818-SL with OD3 neutral density filter). All modulated techniques were also carried out with illumination from a 625 nm LED where appropriate (Thorlabs MRLED). Impedance measurements for different illumination intensities

were made at the corresponding open circuit voltage using an Autolab PGSTAT30. Impedance measurements were also made in the dark as a function of applied voltage. Impedance data were fitted using ZView software (Scribner Associates). IMVS and IMPS measurements were made using a Solartron 1260 frequency response analyzer (FRA) combined with a Thorlabs DC2100 controller (bandwidth 100 kHz) driven by the dc and sine wave output of the FRA. The modulation depth was set to be 10% of the dc level. The illumination intensity was varied using calibrated neutral density filters. To ensure long term stability, cells were illuminated with a single wavelength at intensities of 0.1 Sun and lower. By measuring trends with respect to illumination intensity we were able to derive significant amounts of information on cell behaviour. In the environment solar cells need to operate at illumination intensities below 1 Sun, therefore tests of cell performance at 0.1 Sun can still be considered as the working environment for a cell. To correct for attenuation and phase lag in the modulated light output at higher frequencies, a glass microscope slide was used as a beam splitter enabling provision of a reference signal for the frequency response analyzer from a fast p-i-n photodiode. For IMPS, the cell current was measured using a current amplifier (Femto DLPCA-200). A high impedance (>10^{12} ohm) voltage follower was used for IMVS. The bandwidth of the system was checked using a fast p-i-n photodiode in place of the solar cell. OCVD measurements were made using step function illumination of the cells (625 nm LED; on period 60 s). The voltage decay after switching the light off was measured using the high impedance voltage follower amplifier and a digital storage oscilloscope. Care was taken to totally exclude stray light.

Theory

Diode ideality factor

The diode ideality factor, *n*, is normally defined in terms of the Shockley diode equation, which describes the dependence of the diode current density, *j*, on the applied voltage *V*. Here j_{sat} is the reverse saturation current

$$j = j_{sat}\left(e^{\frac{qV}{nk_BT}} - 1\right) \quad (1)$$

In theory, *n* can take different values between 1 and 3, depending on the recombination mechanism[27] (Hall Shockley Read, Sah Noyce Shockley, Auger etc.), although in some cases anomalously high experimental values of *n* may point to the existence of several junctions in a device.[28] Here we are mainly concerned with the behavior of perovskite cells under illumination, and so we define a diode ideality factor *m* using the intensity dependence of the open circuit voltage, which takes the form

$$\frac{\partial V_{oc}}{\partial \ln I_0} = \frac{mk_BT}{q} \quad (2)$$

The ideality factors, *n* and *m* are not identical for perovskite solar cells since the dark and light current voltage plots cross at forward bias (See ESI).

Impedance

A simple equivalent circuit for a planar thin film p-i-n solar cell is shown in Figure 1. Here the capacitance C_{total} reflects the *overall* charge storage in the device. This is the sum of (a) the charge in the contacts (related linearly to the voltage by the geometric or junction capacitance, C_{geo}) and (b) the charge associated with photogenerated electrons and holes in the perovskite layer (usually related exponentially to the voltage by the chemical capacitance, C_μ). The relationship between C_{geo} and C_μ is discussed in more detail in the main text and also in the supporting information.

Recombination is represented by the voltage-dependent recombination resistance R_{rec}, defined by

$$R_{rec} = \left(\frac{\partial V}{\partial j_{rec}}\right) \quad (3)$$

where j_{rec} is the recombination current density. Generally the variation of the recombination resistance with voltage is related to the ideality factor *m* by

$$\frac{\partial \log R_{rec}}{\partial V} = -\frac{q}{2.303mk_BT} \quad (4)$$

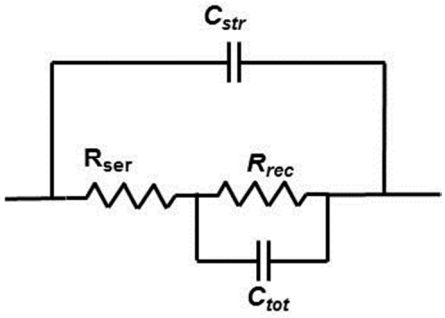

Figure 1. Equivalent circuit of thin film solar cell with elements representing the recombination resistance, R_{rec}, cell capacitance, C_{tot}, series resistance, R_{ser}, and the stray capacitance C_{str}.

R_{ser} is the series resistance of the cell, which in the present case is largely associated with the FTO substrate. C_{total} represents the total capacitance of the cell, $C_{geo} + C_\mu$. If necessary, it can be replaced by constant phase shift elements (CPE) to reflect effects such as those arising from heterogeneity (see supporting information for a discussion of CPE behavior).[29-30] In the case where C_{total} is dominated by the build-up of photogenerated charge (as in the DSC and in silicon p-n devices),[31-32] the recombination lifetime is given by the product of the chemical capacitance C_μ and the recombination resistance R_{rec}. In the case where the geometric capacitance, C_{geo}, dominates the recombination lifetime is not obtained and the time constant for the process is $R_{rec}C_{geo}$.

The circuit shown in Figure 1 neglects complications that arise in the case of perovskite cells from low frequency effects. These have been discussed recently by Bisquert et al.,[26] who attribute the low frequency response to the GDE. Discussion of the low frequency response of the planar cells is deferred to a forthcoming paper. In general,

the circuit model in Figure 1 gives a satisfactory fit of the impedance data for the planar perovskite cells at frequencies above 100 Hz. The low frequency feature only becomes an issue at low light intensities (low open circuit voltages), where the *RC* time constant of the solar cell becomes comparable with the time constant for the process.[29]

The circuit in Figure 1 differs from the transmission line model that has been used for mesoporous perovskite solar cells.[10, 21] As shown below, the planar perovskite cells investigated here do not show transmission line behavior even in the highest frequency part of the impedance responses, indicating that transport of charge carriers by drift/diffusion is very fast in the thin (600 nm) perovskite absorber layer.

IMVS and OCVD

Intensity-modulated photovoltage spectroscopy (IMVS) has been widely used to study recombination in dye-sensitized solar cells (DSC). It has also been used to investigate mesostructured perovskite cells. [33-35] To the best of our knowledge, this is the first time IMVS has been used to characterize *planar* perovskite cells. The method involves using a small sinusoidal modulation of the illumination intensity to perturb the Fermi level splitting around a steady state at open circuit. Generally the IMVS response is a semicircle with a characteristic radial frequency at its maximum that is the inverse of the photovoltage decay time constant, τ_{IMVS}. In the case where the effects of the geometric or junction capacitance can be neglected, τ_{IMVS} is given by the product of the recombination resistance and the chemical capacitance, which corresponds to the ambipolar carrier lifetime. However, in the case where C_{geo} is dominant, we expect τ_{IMVS} to be determined by the product $R_{rec}C_{geo}$.

For open circuit photovoltage decay (OCVD) measurements, the cell is illuminated at open circuit to establish a photostationary state. The light is then switched off and the decay in V_{oc} is monitored as a function of time. The photovoltage decay lifetime, τ_{OCVD}, is then obtained using equation 5 (see ESI).

$$\tau_{OCVD} = -\frac{2k_BT}{q}\left(\frac{dV_{OC}}{dt}\right)^{-1} - \frac{dV_{OC}}{dt}\left(\frac{d^2V_{OC}}{dt^2}\right)^{-1} \qquad (5)$$

Equation 5 is derived using an approach similar to that of Zaban et al. [36], but for the two carrier case where the excess carrier densities are higher than the doping density of the material (see ESI). The second term in equation 5 is often omitted, and a satisfactory approximation of the lifetime can be obtained by the first term (see reference 31 for more details).

If the chemical capacitance of the cell is larger than the geometric capacitance obtained from equation 5, the decay lifetime corresponds to the ambipolar carrier lifetime. However, in the case where the geometric/junction capacitance dominates, we expect τ_{OCVD} to correspond to the *RC* time constant $R_{rec}C_{geo}$.

IMPS

In cases where carrier transport is slow, the IMPS response can be used to measure the delay in collecting carriers at the contacts. IMPS has been used extensively to study trap-limited electron transport in dye-sensitized solar cells.[37-38] It has also been used to study mesostructured perovskite solar cells.[33] However, in the case of normal p-n or p-i-n solar cells without deep trap states, carrier separation is so fast that it is much more difficult to measure by IMPS. The high frequency IMPS response is dominated in this case by the attenuation arising from the time constant of the solar cell, which corresponds to $R_{ser}C_{total}$ in Figure 1. By contrast, in the case of mesostructured perovskite solar cells, IMPS may give both the RC time constant and a time constant due to electron transport in the mesoporous titania scaffold. IMPS has also been used to characterize charge transfer and recombination in semiconductor-electrolyte contacts. [38,39] In this case, the modulated illumination generates a flux of minority carriers into the surface (e.g. at the semiconductor – solution interface). Once there, the carriers can either be involved in a charge transfer reaction or they may combine with majority carriers. The relaxation of the minority carrier concentration at the surface by charge transfer and recombination gives rise to a semicircle in the complex plane IMPS plot with a radial frequency at the maximum that is equal to the inverse of the relaxation lifetime $\tau_{IMPS}^{-1} = k_{trans} + k_{rec}$. The normalized low frequency intercept of the IMPS plot corresponds to the dc response, and it depends on the fraction of the minority carriers that make it across the interface. This *charge transfer efficiency*, η_{trans} is given simply by the ratio $k_{trans}/(k_{trans} + k_{rec})$.[39-40] Here k_{trans} and k_{rec} are first order (or pseudo first order) rate constants for charge transfer and recombination at short circuit respectively.

Results and Discussion

Cell Efficiencies

Representative IV curves (Fig. S1 and S2) and a summary of the efficiencies of all the cells used in this study is given in the supporting information. Five devices were studied, each of which contained three pixels, making a total of fifteen solar cells. The cells showed an average efficiency of 11.05% at 1 sun and AM1.5 with a standard deviation of 1.02% (number of samples, n=14).The two cells presented in most detail below had efficiencies of 11.98% (FS43_1) and 9.60% (FB06_1). One of the pixels gave an anomalously low efficiency and was disregarded, two further pixels degraded during transport and the data from them was also not included in the study.

Intensity dependence of V_{oc}

All of the cells were made at the same time using identical techniques and were annealed together on the same hotplate. Figure 2 illustrates the two types of intensity dependence of the open circuit voltage observed when the cells were illuminated with monochromatic light (λ= 625 nm). Interestingly the cells fell into two groups. Five of the twelve cells measured showed ideality factors around 2.6 (average = 2.61; std dev = 0.09) and 7 showed

ideality factors of around 5.2 (average = 5.20; std dev = 0.31). Pixels on the same device always gave similar ideality factors, with three out of the five devices showing higher ideality factors and two showing lower ones.

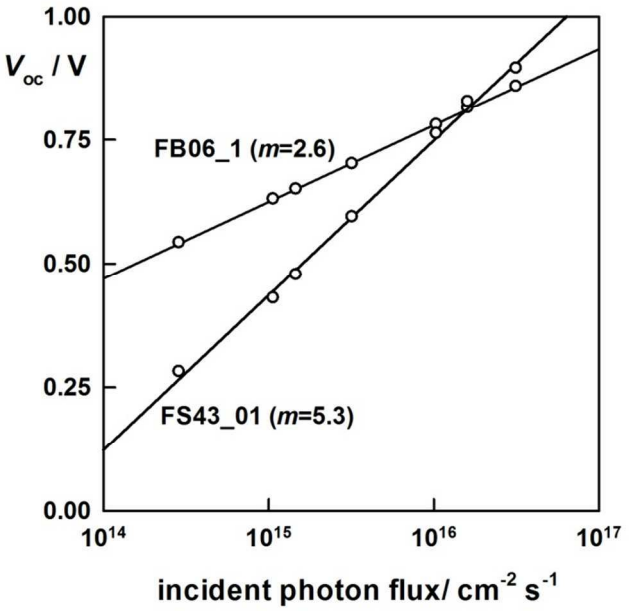

Figure 2. Intensity dependence of the open circuit voltages for two different cells/pixels illustrating the difference in ideality factor between the two groups.

Interestingly, the cell with the higher ideality factor (m=5.3) gives a higher open circuit voltage at the highest photon flux (3.17×10^{16} cm^{-2} s^{-1}), which in terms of the measured short circuit currents is equivalent to 0.1 sun AM 1.5 illumination. However, V_{oc} for this type of cell falls rapidly as the intensity is decreased so that the plots cross at the equivalent of 0.03 suns (1.61×10^{15} cm^{-2} s^{-1}). The reason for the differences in ideality between two sets of cells made under identical conditions is unknown. We suggest that differences in the annealing temperature due to a small temperature gradient on the hotplate could be responsible. The size and composition of the perovskite crystallites has been shown to be rather dependent on small changes in preparation techniques.[41] In addition other authors have found two types of behaviour for perovskite films that are deposited under identical conditions. Zaban et al[42] observed two distinct types of behaviour for perovskite films sandwiched between gold electrodes, they attributed the differences to the specific structure or orientation of the polycrystalline film with respect to the gold electrodes. We could not find any other literature examples where the ideality factors from V_{oc} versus intensity data for perovskite cells have been reported.

Open Circuit Voltage Decay and IMVS

Experimental OCVD decay plots for the cells are shown in Figure 3. Again two distinct types of behaviour were observed. It can be seen that the cell with m=2.6 in Figure 2 exhibits a remarkably slow decay of V_{oc}: the voltage is still 0.4 V after 1 second, and the decay is not complete even at 10 s. By contrast, the open circuit voltage of the cell with m=5.3 decays much more rapidly, falling below 0.1 V in only 10 ms. Similar anomalously slow OCVD behavior has been reported by Baumann et al.[25] for vapor-deposited perovskite cells in which the TiO2 and MeOTAD contacts were replaced by $PC_{70}PCBM$ and PEDOT:PSS/polyTPD respectively. The authors interpreted the decay in terms of the kinetics of electron-hole recombination and found that the recombination order was between 2 and 3 and that it varied depending on the illumination intensity the cell was exposed to prior to the decay.

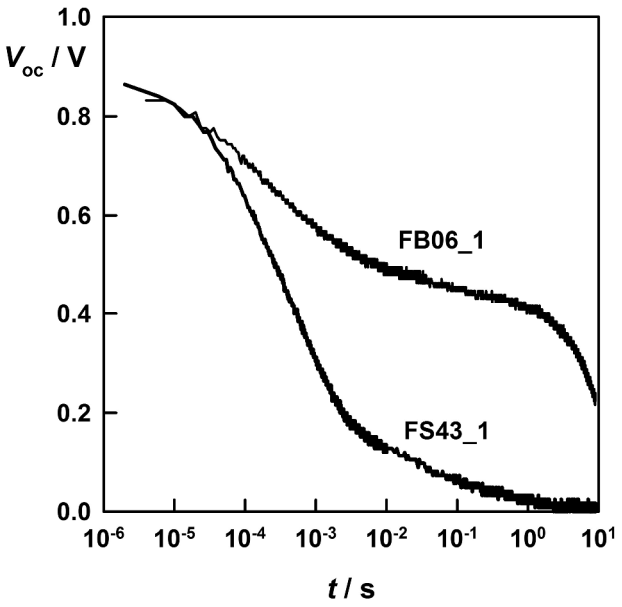

Figure 3. Open circuit voltage decays for the two types of cell. Note that the cell with the lower m value in Figure 2 (FB-06_1) exhibits the anomalously slow voltage decay, whereas the voltage of cell with m = 5.3 decays much more rapidly.

The IMVS responses (Figure S8 shows representative IMVS data) of the cells measured over two decades of light intensity were well-defined semicircles in the complex plane, and τ_{IMVS} was derived from the inverse of the radial frequency corresponding to the maximum of the imaginary component.

The lifetimes derived from the OCVD plots in Figure 3 and from the corresponding IMVS measurements on the two representative cells are presented in Figure 4. Details of the smoothing and fitting procedures used to obtain τ_{OCVD} are given in the supporting information. The reasonable agreement between the lifetimes derived by the transient and small sinusoidal modulation methods indicates that the open circuit decays through a set of quasistatic states, at least in the voltage range preceding the steeper rise in lifetime that can be seen in the τ plots for both cells. The slopes of the regression fits of the IMVS plots for the two types of cell correspond to m values which are similar to those derived from the intensity dependence of the open circuit voltage (cf. Figure 2). It is

important to note that as the geometric capacitance dominates the response of the planar cells (see EIS discussion in the next section), OCVD and IMVS are not measuring the time constant for ambipolar recombination. The relaxation time, τ_{IMVS}/τ_{OCVD}, instead appears to be dictated by the product $R_{rec}C_{geo.}$

The lifetimes measured by IMVS for the two cells were found to be inversely proportional to the incident light intensity as shown in Figure 5. Remarkably, the lifetimes of the two cells at the same light intensity are very similar, in spite of the fact that the open circuit voltages (and presumably therefore the excess electron and hole concentrations) are quite different. As shown below, the recombination resistances of the two cells measured by impedance spectroscopy were also very similar when measured at the same illumination intensity (cf. Figure 8). The recombination resistance is expected to vary linearly with the inverse of light intensity, providing the dark and light responses from the cell are additive (see supporting information). As the lifetime τ_{IMVS}/τ_{OCVD}, equals $R_{rec}C_{geo}$ in the case of the cells measured here, it follows that τ_{IMVS}/τ_{OCVD} should also vary linearly with light intensity provided that C_{geo} is effectively constant across the full range of light intensities measured. This contrasts strongly with the case of normal p-n junctions, where the chemical capacitance is dominant and increases with light intensity due to the increase in electron and hole concentrations.

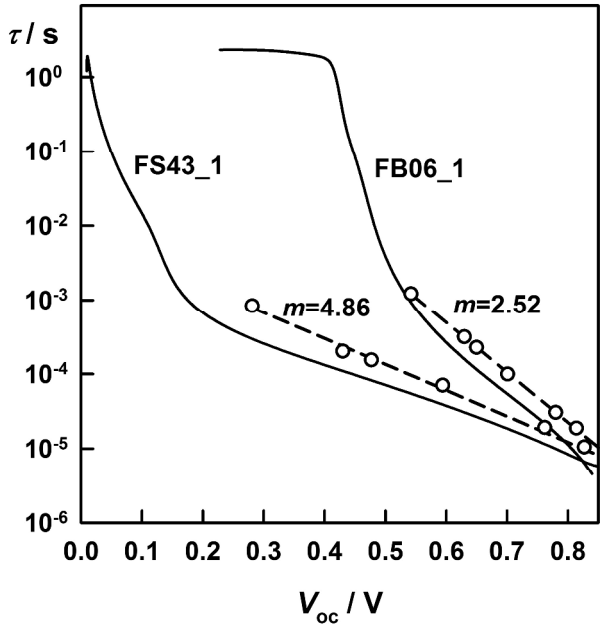

Figure 4. Lifetimes (τ_{IMVS} and τ_{OCVD}) for the two cells derived from the open circuit voltage decay (lines) and from the IMVS response (open circles). The regression fits of the IMVS lifetimes give the values of m shown on the figure. These are similar to those derived from the intensity dependence of the V_{oc} (see Figure 2).

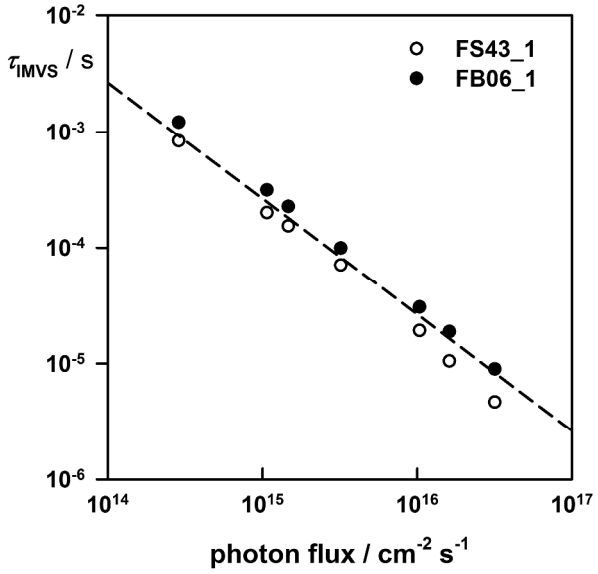

Figure 5. Intensity dependence of the lifetimes measured by IMVS for the two cells. The broken line corresponds to a linear dependence (slope = -1).

Impedance

Impedance measurements were carried out at open circuit under illumination (and also in the dark as a function of voltage bias - see ESI). Figures 6a and 6b illustrate the impedance response observed at an intensity corresponding to ~0.1 sun. At all intensities three typical features were seen in the Nyquist plots. A mid frequency semi-circle was attributed to C_{total} and R_{rec}. The semi-circle was distorted at the highest frequencies by another process which we have attributed the effect of stray capacitance (e.g. from the connectors); however it could also be due to the impedance of the titania blocking layer. A third low frequency feature was always observed below ~100Hz as illustrated in figure 6a. Each of the features is discussed in more detail below.

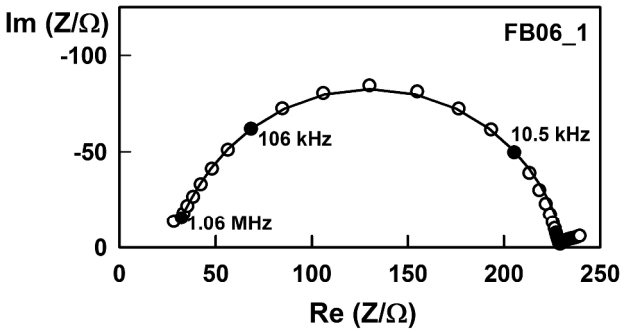

Figure 6a. Example of the impedance response measured at open circuit at the highest light intensity (λ = 625 nm, 3.17 × 10^{16} cm^{-2} s^{-1}). Points experimental, line fitting to the circuit shown in Figure 1.

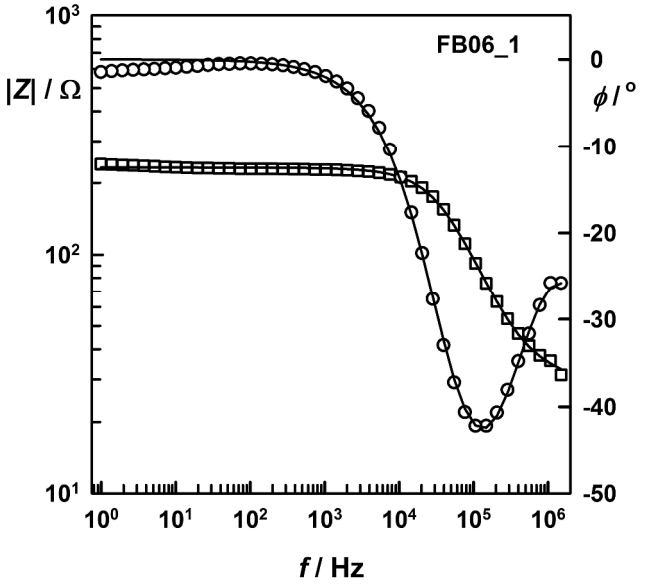

Figure 6b Bode plot (symbols) and fit (lines) to the circuit shown in Figure 1 with C_{jun} replaced by a constant phase shift element for the impedance response shown in Figure 6b.

Impedance measurements have been used extensively to characterize mesostructured lead halide perovskite solar cells.[10, 22, 24] In the case of the mesostructured cells, the analysis has been based on transmission line models developed for dye-sensitized solar cells that consider electron transport and recombination.[10, 13, 21, 26, 43] In the case of the planar perovskite cells studied here, we did not observe transmission line behavior, even at the highest frequencies (1.5 MHz). It is likely therefore, that for these planar cells the transport of carriers through the perovskite films is too fast to be measured by impedance spectroscopy. This result suggests that the response of these planar cells is much simpler than that of mesostructured cells, and it is possible that the transmission line seen in mesostructured cells is a result of the electrons in the titania scaffold rather than in the perovskite itself.

The time constant for the semi-circle obtained in the impedance of all the planar cells, at all illumination intensities, was much shorter than the relaxation time reported for the giant dielectric effect. [12,36,13, 26] The response can be fitted to the simple circuit shown in Figure 1 if the total capacitance is replaced by a constant phase shift element. When this was done the P-values for the CPE representing C_{total} were all between 0.87 and 1 (see ESI for further discussion). It should also be noted that fitting the mid frequency range of the semi-circle to a simple model containing only R_{ser}, R_{rec}, C_{total} without a CPE gave a reasonable fit and showed identical trends in the recombination resistance. When the simple $R_{ser}(R_{rec}C_{total})$ model was used, C_{total} (e.g. reported here for FS43_1) had values of between 20 and 32 nF over the entire intensity (and hence voltage) range. The geometric capacitance for a perfectly smooth device can be calculated to be ~ 5.3 nF ($C = \varepsilon_o\varepsilon_r A/d$; A=0.15cm^2, d=600nm, ε_r = 24[12, 44]). The experimentally derived values of the capacitance are approximately 4 times larger than the calculated geometric capacitance for the cell using a relative permittivity of 24. This suggests either a perfectly flat perovskite film with a relative permittivity of 100 or a film with a relative permittivity of 24 and a roughness factor of 4. A roughness factor of 4 is entirely reasonable for a multi-crystalline perovskite film; mechanically polished gold films have roughness factors of between 3 and 5 for example.[45] However the difference in calculated and measured capacitance could also be due to an increase in dielectric constant under illumination as reported by Juarez-Perez et al.[13]

The impedance results strongly suggests that C_{total} is dominated by the value of the geometric capacitance and that the charge stored in the contacts is significantly larger than the charge due to photogenerated electrons and holes in the perovskite. In contrast to measurements on mesostructured cells with titania scaffolds, we do not appear to measure the chemical capacitance and do not see large amounts of charge stored in the bulk of the perovskite.[13, 33] Previous measurements on planar perovskite cells (300nm active layer) also showed a large capacitance which was attributed to a high intrinsic density of states in perovskite films.[21] We did not observe such a large capacitance in our measurements, and the devices studied here show a capacitance which does not vary strongly with intensity. It is possible that the capacitance behavior depends on the methods used to prepare the perovskite cells, as several recent papers have shown large differences in cell properties for small differences in preparation techniques.[46-48] The fact that C_g dominates C_μ over the frequency range is consistent with a p-i-n device, although other authors have suggested that perovskite solar cells may function as p-n devices.[49]

The parallel resistance that accompanies C_{geo} is attributed to the recombination resistance. The lifetimes calculated from the product of C_{geo} and R_{rec} agree well with the values measured by IMVS and OCVD (Fig 4 and Fig S9). We therefore conclude that the perovskite can be considered as essentially intrinsic. This is consistent with the very low doping density (~10^9 cm^{-3}) calculated from the transition to first order decay seen in Figure 4. The variations of the recombination resistance with V_{oc} and with intensity are shown in Figure 7 and Figure 8. The semilogarithmic plots of R_{rec} vs. V_{oc} for the two types of cell have different slopes as shown in Figure 7, reflecting the different ideality factors of the cells. The ideality factors of 2.7 and 4.8 are very similar to those obtained from the intensity dependence of the open circuit voltage (cf. Figure 2). By contrast, the intensity dependence of R_{rec} is almost identical for both types of cell, with a slope close to -1, mirroring the intensity dependence of τ_{IMVS} measured by IMVS (cf. Figure 5).

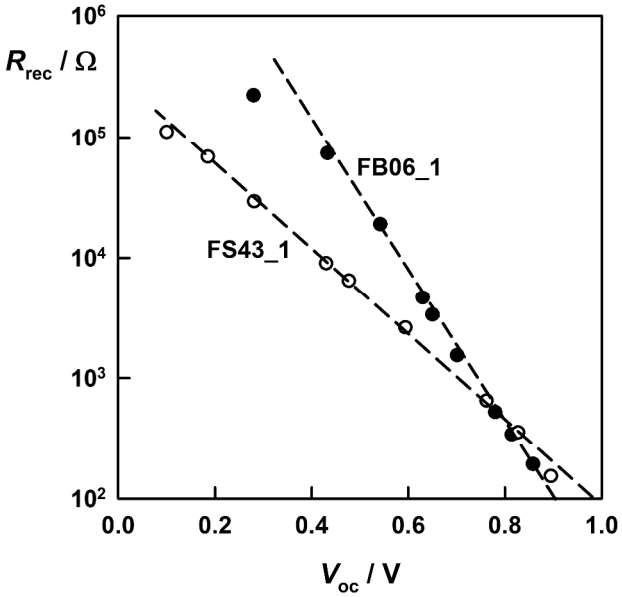

Figure 7. Recombination resistance for the two different types of cell measured at open circuit under different illumination intensities. The slopes of the lines shown are 281 mV/decade for FS43-1 and 161 mV/decade for FB-06, corresponding to m values of 4.8 and 2.7 respectively.

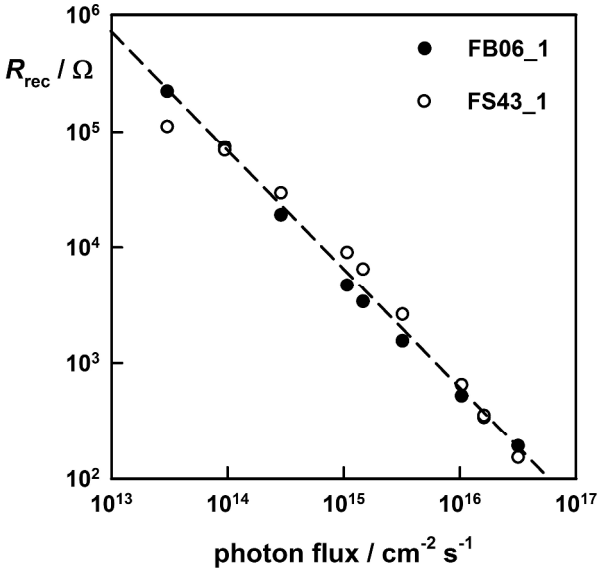

Figure 8. Intensity dependence of the recombination resistance for the two cells. The broken line corresponds to a linear dependence of R_{rec} on incident photon flux.

The low frequency feature that appears in the impedance plots below 100Hz has not been studied in detail, as we were concerned that the cells could degrade on the timescale of the very slow low frequency measurements. Juarez-Perez et al. attribute the low frequency feature to the GDE in the perovskite.[13] We are currently looking at the low frequency feature in more detail, but the conclusion of this paper is that a simple circuit gives a good fit to all data above 100Hz.

IMPS

IMPS has been extensively used to investigate carrier transport in DSC. It has also been used to study recombination and interfacial transfer of minority carriers in illuminated semi-conductor electrodes.[39-40, 50] IMPS was recently used by Guillén et al. to study mesostructured perovskite cells; two time constants were observed in one quadrant of the complex plane plot. Figure 9 shows a representative IMPS plot for FS43_1 at 0.1 sun equivalent illumination. The high frequency semi-circle is incomplete as the LED could not be modulated satisfactorily at frequencies higher than 200 kHz. The IMPS response for DSC is usually a semicircle trending to a 45° line towards the origin at high frequencies. The characteristic frequency of the semi-circle is related to the electron transport time, which ranges from ms to s, depending on the illumination intensity. By contrast, in the case of the planar perovskite solar cells studied here, the high frequency semi-circle is dominated by the time constant $R_{ser}C_{geo}$ of the cell, and it is difficult to deconvolute the effect of carrier transport because the carrier transit times are similar to or shorter than the *RC* time constant. However, we believe that the distortion of the semicircle at high frequencies may not be an instrumental artefact but could be due to an additional phase lag associated with transport. The values of the series resistance measured by impedance spectroscopy were used to estimate the capacitance from the relaxation time for the high frequency semi-circle. The series resistance for FB06_1, for example, was ~40Ω, which gave capacitance values of between 26 and 36 nF. These values are consistent with the values of C_{total} obtained from both IMVS and impedance spectroscopy.

Interestingly a second semi-circle in the lower quadrant is seen at lower frequencies. As discussed above, a similar response is observed for illuminated semiconductor/electrolyte junctions, where the second semi-circle is due to the relaxation of the minority carrier concentration at short circuit by charge transfer (with rate k_{trans}) and recombination (with rate k_{rec}) at the solution-electrode interface. The high frequency intercept corresponds to the instantaneous photocurrent and the low frequency limit to the steady state photocurrent. In this case, the semi-circle has a radial frequency at the minimum that is equal to the inverse of the relaxation lifetime $\tau_{IMPS}^{-1} = k_{trans} + k_{rec}$, and a normalized low frequency intercept that depends on the charge transfer efficiency, $\eta_{trans} = k_{trans}/(k_{trans} + k_{rec})$. It should be noted that the 'relaxation lifetime' measured using IMPS is quite separate from the 'recombination lifetime' which is measured at open circuit. The open circuit recombination lifetime is the product of the chemical capacitance and the recombination resistance. In contrast, the relaxation lifetime from IMPS is measured at short circuit. The IMPS lifetime is not influenced by the geometric capacitance which, as outlined above, is observed in the high frequency semi-circle in the upper quadrant of the IMPS plot. IMPS can therefore give useful information about interfacial charge transport and recombination in perovskite solar cells at short circuit.

In view of the similarity mentioned above, we attribute the low frequency IMPS response for the perovskite cells to the relaxation of photogenerated carriers due interfacial recombination and transport at short circuit. Values for k_{trans}, k_{rec}, τ_{IMPS} and η_{trans} were extracted from the maximum frequency and normalized low frequency intercepts of the IMPS plots recorded as a function of light intensity. Figure 10 shows the collection efficiency, η_{trans}, for the two cells studied in detail in this paper. It can be seen that η_{trans} for FS43_1 is higher

than that of FB06_1 at all intensities. This result is consistent with the higher global efficiency measured for this cell.

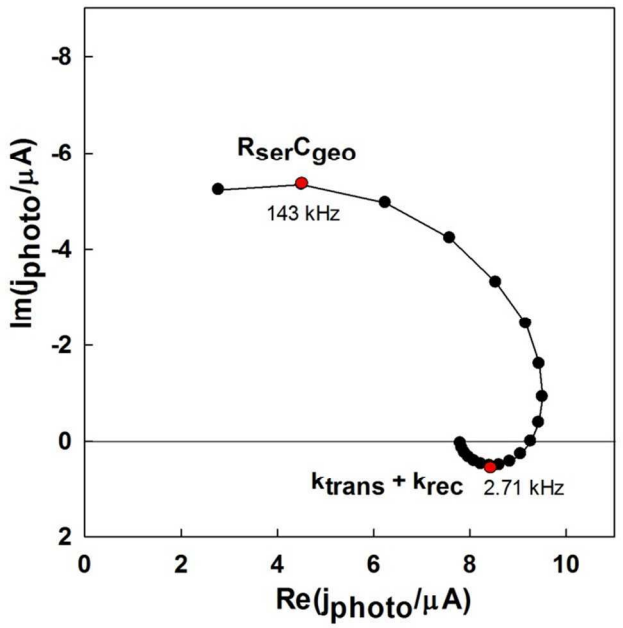

Figure 9. IMPS response for FS43_1 showing the RC time constant at high frequency and a low frequency semi-circle which is related to transport and recombination.

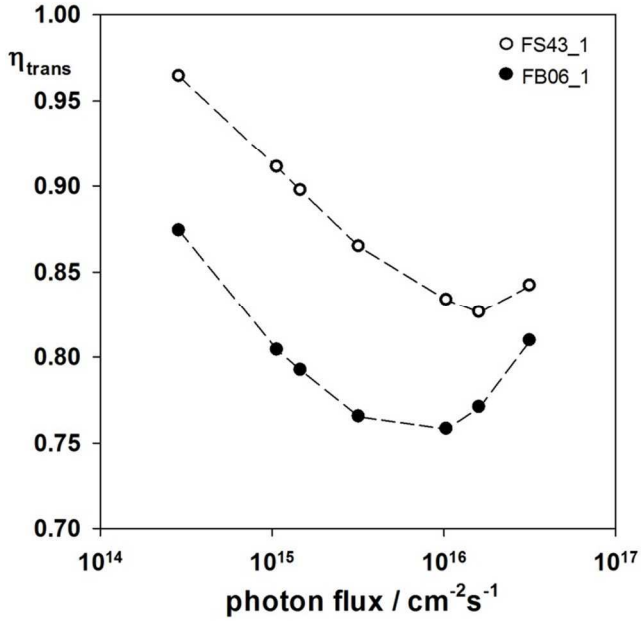

Figure 10. Collection efficiency, η_{trans}, for FB06_1 and FS43_1 calculated from the intercept of the low frequency semi-circle in the IMPS.

Figure 11 shows the short circuit relaxation lifetime calculated from the maximum of the low frequency IMPS semi-circles. A linear variation with intensity is seen for τ_{IMPS} and its values are higher than the values of τ_{IMVS} measured at the same light intensities. The calculated rate constants are shown in Figure 12. At all intensities k_{trans} is approximately an order of magnitude greater than k_{rec} which is consistent with the high external quantum efficiencies typically measured for perovskite solar cells under short circuit conditions. Cell FB06_1 showed a higher recombination rate than cell FS43_1 (3.43 x 10^3 s^{-1} compared to 3.18 x 10^3 s^{-1} at 0.1 sun); the rate constant for interfacial transport was also slower (1.46 x 10^4 s^{-1} compared to 1.69 x $10^4 s^{-1}$). The differences between the cells increased at lower illumination levels. This data is consistent with the lower short circuit current observed for FB06_1. The variation in η_{trans} with intensity is due to the changes in k_{trans} *and* k_{rec} with intensity. The data in Fig. 11 is not linear with intensity, with k_{trans} increasing and k_{rec} decreasing as the light intensity is decreased.

Further work is in progress to relate the rate constants derived from the IMPS measurements to models of surface recombination.

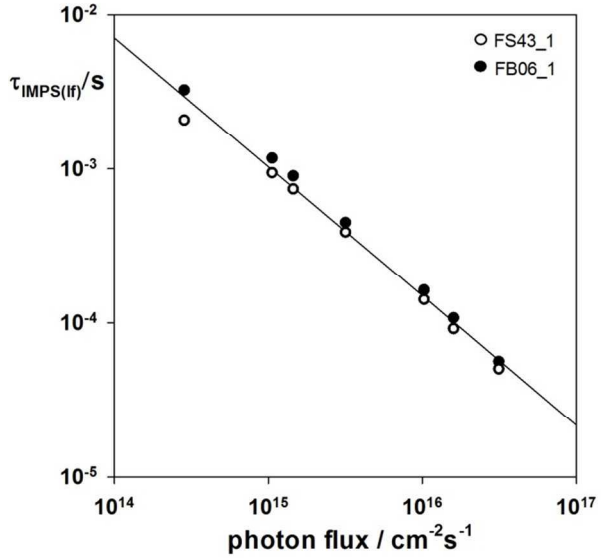

Figure 11. τ_{IMPS} from IMPS measurements of FB06_1 and FS43_1.

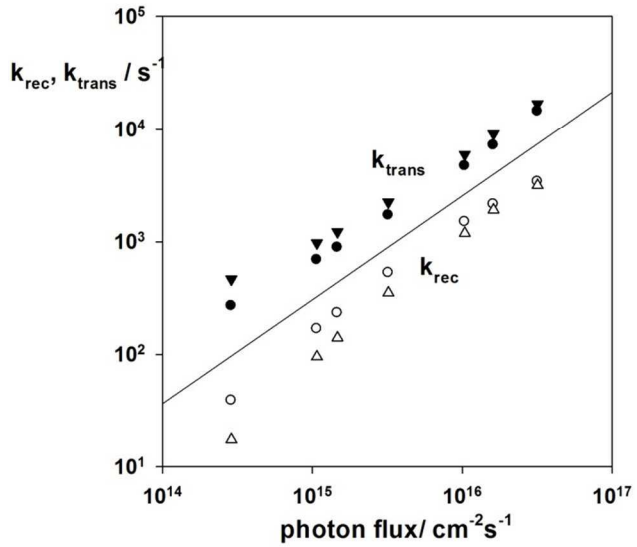

Figure 12. Recombination rate constant (open symbols) and transport rate constant (solid symbols) as a function

of intensity. The circles show data for FB06_1 and the triangles for FS43_1.

Conclusions

IMVS, OCVD, impedance and IMPS have been used to study planar perovskite solar cells. Despite the fact that all the cells were made at the same time, two distinct sets of behaviours were seen. Half the cells had ideality factors of ~2.6 and the other half showed ideality factors of ~5.2.The difference in behavior was also seen in the OCVD: the cells with the lower ideality factors showed a persistent photovoltage. Lifetimes from IMVS were in good agreement with those calculated from OCVD. IMVS and impedance spectroscopy showed time constants that were dominated by the geometric capacitance rather than the chemical capacitance, meaning that the ambipolar recombination lifetime could not be extracted. IMPS showed two semi-circles, one at high frequency attributed to the RC time constant of the cells and a second at lower frequency attributed to interfacial transport and recombination at short circuit. Analysis of the IMPS response suggests that the collection of photogenerated carriers is very efficient under short circuit conditions in these planar perovskite cells

AUTHOR INFORMATION

Corresponding Author

*Email: p.j.cameron@bath.ac.uk; l.m.peter@bath.ac.uk;
Tel: +44 (0)1225 386116.

Author Contributions

The manuscript was written through contributions of all authors. All authors have given approval to the final version of the manuscript.

Funding Sources

EPSRC (EP/G031088/1; EP/F047819/1, EP/G03768X/1) and European Union Seventh Framework Programme [FP7/2007-2013] under grant agreement 316494.

ACKNOWLEDGMENT

The authors thank Aron Walsh, Jarvist Frost, Christopher Eames and Saiful Islam for helpful discussions. PJC thanks the EPSRC for funding (EP/G031088/1; EP/F047819/1 and DTC studentship for Adam Pockett, Grant EP/G03768X/1). The research leading to these results has received funding from the European Union Seventh Framework Programme [FP7/2007-2013] under grant agreement 316494.

ASSOCIATED CONTENT

Supporting Information contains IV characteristics and cell efficiencies, IMVS results, analysis of constant phase shift elements, dark impedance, OCVD fitting and theory and modelling of the geometric and chemical capacitance for a planar p-i-n cell. This information is available free of charge via the Internet at http://pubs.acs.org

SYNOPSIS TOC. Planar perovskite solar cells have been characterized by impedance spectroscopy (IS), IMVS, IMPS and OCVD. The cells fell into two groups; one group that showed ideality factors of ~2.6 and one groups that showed ideality factors of >5. In contrast to published results for mesostructured perovskite solar cells, the IMVS and IS response for planar cells was dominated by the geometric capacitance of the devices. Electron diffusion was too fast to be observed in either IS or IMPS. Interestingly IMPS showed a feature which has been attributed to interfacial transport and recombination at short circuit and suggests collection efficiencies >80% in the ~12% efficient planar perovskite cells.

REFERENCES

(1) Liu, M.; Johnston, M. B.; Snaith, H. J. Efficient Planar Heterojunction Perovskite Solar Cells by Vapour Deposition. *Nature* **2013**, *501*, 395-398.

(2) Lee, M. M.; Teuscher, J.; Miyasaka, T.; Murakami, T. N.; Snaith, H. J. Efficient Hybrid Solar Cells Based on Meso-Superstructured Organometal Halide Perovskites. *Science* **2012**, *338*, 643-647.

(3) Etgar, L.; Gao, P.; Xue, Z.; Peng, Q.; Chandiran, A. K.; Liu, B.; Nazeeruddin, M. K.; Grätzel, M. Mesoscopic CH3NH3PbI3/Tio2 Heterojunction Solar Cells. *J. Am. Chem. Soc.* **2012**, *134*, 17396–17399.

(4) Kim, H.-S.; Lee, C.-R.; Im, J.-H.; Lee, K.-B.; Moehl, T.; Marchioro, A.; Moon, S.-J.; Humphry-Baker, R.; Yum, J.-H.; Moser, J. E., et al. Lead Iodide Perovskite Sensitized All-Solid-State Submicron Thin Film Mesoscopic Solar Cell with Efficiency Exceeding 9%. *Sci. Rep.* **2012**, *2*, 591.

(5) Bretschneider, S. A.; Weickert, J.; Dorman, J. A.; Schmidt-Mende, L. Research Update: Physical and Electrical Characteristics of Lead Halide Perovskites for Solar Cell Applications. *APL Mat.* **2014**, *2*, 040701.

(6) Ryu, S.; Noh, J. H.; Jeon, N. J.; Kim, Y. C.; Yang, W. S.; Seo, J. W.; Seok, S. I. Voltage Output of Efficient Perovskite Solar Cells with High Open-Circuit Voltage and Fill Factor. *Energy Environ. Sci.* **2014**, *7*, 2614-2618.

(7) Wehrenfennig, C.; Eperon, G. E.; Johnston, M. B.; Snaith, H. J.; Herz, L. M. High Charge Carrier Mobilities and Lifetimes in Organolead Trihalide Perovskites. *Adv. Mater.* **2014**, *26*, 1584-1589.

(8) Yin, W.-J.; Shi, T.; Yan, Y. Unique Properties of Halide Perovskites as Possible Origins of the Superior Solar Cell Performance. *Adv. Mater.* **2014**, *26*, 4653-4658.

(9) Ponseca, C. S.; Savenije, T. J.; Abdellah, M. A.; Zheng, K.; Yartsev, A. P.; Pascher, T.; Harlang, T.; Chabera, P.; Pullerits, T.; Stepanov, A., et al. Organometal Halide Perovskite Solar Cell Materials Rationalized – Ultrafast Charge Generation, High and Microsecond-Long Balanced Mobilities and Slow Recombination. *J. Am. Chem. Soc.* **2014**, *136*, 5189-5192.

(10) Gonzalez-Pedro, V.; Juarez-Perez, E. J.; Arsyad, W.-S.; Barea, E. M.; Fabregat-Santiago, F.; Mora-Sero, I.; Bisquert, J. General Working Principles of CH3NH3PbX3 Perovskite Solar Cells. *Nano Lett.* **2014**, *14*, 888-893.

(11) Frost, J. M.; Butler, K. T.; Brivio, F.; Hendon, C. H.; van Schilfgaarde, M.; Walsh, A. Atomistic Origins of High-Performance in Hybrid Halide Perovskite Solar Cells. *Nano Lett.* **2014**, *14*, 2584-2590.

(12) Frost, J. M.; Butler, K. T.; Walsh, A. Molecular Ferroelectric Contributions to Anomalous Hysteresis in Hybrid Perovskite Solar Cells. *APL Mat.* **2014**, *2*, 081506.

(13) Juárez-Pérez, E. J.; Sánchez, R. S.; Badia, L.; Garcia-Belmonte, G.; Kang, Y. S.; Mora-Sero, I.; Bisquert, J. Photoinduced Giant Dielectric Constant in Lead Halide Perovskite Solar Cells. *J. Phys. Chem. Lett.* **2014**, *9*, 2390-2394.

(14) Zhou, H.; Chen, Q.; Li, G.; Luo, S.; Song, T.-b.; Duan, H.-S.; Hong, Z.; You, J.; Liu, Y.; Yang, Y. Interface Engineering of Highly Efficient Perovskite Solar Cells. *Science* **2014**, *345*, 542-546.

(15) Savenije, T. J.; Ponseca, C. S.; Kunneman, L. T.; Abdellah, M. A.; Zheng, K.; Tian, Y.; Zhu, Q.; Canton, S. E.; Scheblykin, I. G.; Pullerits, T., et al. Thermally Activated Exciton Dissociation and Recombination Control the Organometal Halide Perovskite Carrier Dynamics. *J. Phys. Chem. Lett.* **2014**, *5*, 2189–2194.

(16) Marchioro, A.; Teuscher, J.; Friedrich, D.; Kunst, M.; van de Krol, R.; Moehl, T.; Grätzel, M.; Moser, J.-E. Unravelling the Mechanism of Photoinduced Charge Transfer Processes in Lead Iodide Perovskite Solar Cells. *Nat. Photon.* **2014**, *8*, 1-6.

(17) Wehrenfennig, C.; Liu, M.; Snaith, H. J.; Johnston, M. B.; Herz, I. Charge-Carrier Dynamics in Vapour-Deposited Films of the Organolead Halide Perovskite CH3NH3PbI3−xClx. *Energy Environ. Sci.* **2014**, 2269-2275.

(18) Stranks, S. D.; Eperon, G. E.; Grancini, G.; Menelaou, C.; Alcocer, M. J. P.; Leijtens, T.; Herz, L. M.; Petrozza, A.; Snaith, H. J. Electron-Hole Diffusion Lengths Exceeding 1 Micrometer in an Organometal Trihalide Perovskite Absorber. *Science* **2013**, *342*, 341-344.

(19) Edri, E.; Kirmayer, S.; Henning, A.; Mukhopadhyay, S.; Gartsman, K.; Rosenwaks, Y.; Hodes, G.; Cahen, D. Why Lead Methylammonium Tri-Iodide Perovskite-Based Solar Cells Require a Mesoporous Electron Transporting Scaffold (but Not Necessarily a Hole Conductor). *Nano Lett.* **2014**, *14*, 1000-1004.

(20) Abate, A.; Saliba, M.; Hollman, D. J.; Stranks, S. D.; Wojciechowski, K.; Avolio, R.; Grancini, G.; Petrozza, A.; Snaith, H. J. Supramolecular Halogen Bond Passivation of Organic-Inorganic Halide Perovskite Solar Cells. *Nano Lett.* **2014**, 3247–3254.

(21) Kim, H.-S.; Mora-Sero, I.; Gonzalez-Pedro, V.; Fabregat-Santiago, F.; Juarez-Perez, E. J.; Park, N.-G.; Bisquert, J. Mechanism of Carrier Accumulation in Perovskite Thin-Absorber Solar Cells. *Nat. Commun.* **2013**, *4*, 2242.

(22) Dualeh, A.; Moehl, T.; Tétreault, N.; Teuscher, J.; Gao, P.; Nazeeruddin, M. K.; Grätzel, M. Impedance Spectroscopic Analysis of Lead Iodide Perovskite-Sensitized Solid-State Solar Cells. *ACS nano* **2014**, *8*, 362-373.

(23) Sanchez, R. S.; Gonzalez-Pedro, V.; Lee, J.-W.; Park, N.-G.; Kang, Y. S.; Mora-Sero, I.; Bisquert, J. Slow Dynamic Processes in Lead Halide Perovskite Solar Cells. Characteristic Times and Hysteresis. *J. Phys. Chem. Lett.* **2014**, *5*, 2357-2363.

(24) Suarez, B.; Gonzalez-Pedro, V.; Ripolles, T. S.; Sánchez, R. S.; Otero, L. A.; Mora-Sero, I. Recombination Study of Combined Halides (Cl, Br, I) Perovskite Solar Cells. *J. Phys. Chem. Lett.* **2014**, *5*, 1628–1635.

(25) Baumann, A.; Tvingstedt, K.; Heiber, M. C.; Väth, S.; Momblona, C.; Bolink, H. J.; Dyakonov, V. Persistent Photovoltage in Methylammonium Lead Iodide Perovskite Solar Cells. *APL Mat.* **2014**, *2*, 081501.

(26) Bisquert, J.; Bertoluzzi, L.; Mora-Sero, I.; Garcia-Belmonte, G. Theory of Impedance and Capacitance Spectroscopy of Solar Cells with Dielectric Relaxation, Drift-Diffusion Transport, and Recombination. *J. Phys. Chem. C* **2014**, *118*, 18983-18991.

(27) Landsberg, P. T. *Recombination in Semiconductors*; Cambridge University Press: Cambridge, UK, 1991.

(28) Shah, J. M.; Li, Y.-L.; Gessmann, T.; Schubert, E. F. Experimental Analysis and Theoretical Model for Anomalously High Ideality Factors (N≫2.0) in AlGaN/GaN P-N Junction Diodes. *J. Appl. Phys.* **2003**, *94*, 2627-2630.

(29) Brug, G. J.; van den Eeden, A. L. G.; Sluyters-Rehbach, M.; Sluyters, J. H. The Analysis of Electrode Impedances Complicated by the Presence of a Constant Phase Element. *J. Electroanal. Chem. Interfac.* **1984**, *176*, 275-295.

(30) Hirschorn, B.; Orazem, M. E.; Tribollet, B.; Vivier, V.; Frateur, I.; Musiani, M. Constant-Phase-Element Behavior Caused by Resistivity Distributions in Films. In *Corrosion*, Hansen, D. C.; Alfantazi, A.; Gelling, V. J., Eds. 2010; Vol. 28, pp 77-94.

(31) Mora-Sero, I.; Garcia-Belmonte, G.; Boix, P. P.; Vazquez, M. A.; Bisquert, J. Impedance Spectroscopy Characterisation of Highly Efficient Silicon Solar Cells under Different Light Illumination Intensities. *Energy Environ. Sci.* **2009**, *2*, 678-686.

(32) Bisquert, J. Theory of the Impedance of Electron Diffusion and Recombination in a Thin Layer. *J. Phys. Chem. B* **2001**, *106*, 325-333.

(33) Guillén, E.; Ramos, F. J.; Anta, J. A.; Ahmad, S. Elucidating Transport-Recombination Mechanisms in Perovskite Solar Cells

by Small-Perturbation Techniques. *J. Phys. Chem. C* **2014**, *118*, 22913–22922.
(34) Zhao, Y.; Nardes, A. M.; Zhu, K.. Mesoporous Perovskite Solar Cells: Material Composition, Charge-Carrier Dynamics, and Device Characteristics. *Farad. Discuss.* **2014**, Advance article.
(35) Zhao, Y.; Nardes, A. M.; Zhu, K.. Solid-State Mesostructured Perovskite CH3NH3PbI3 Solar Cells: Charge Transport, Recombination, and Diffusion Length. *J. Phys. Chem. Lett.* **2014**, *5*, 490-494.
(36) Zaban, A.; Greenshtein, M.; Bisquert, J. Determination of the Electron Lifetime in Nanocrystalline Dye Solar Cells by Open-Circuit Voltage Decay Measurements. *ChemPhysChem* **2003**, *4*, 859-864.
(37) Franco, G.; Peter, L. M.; Ponomarev, E. A. Detection of Inhomogeneous Dye Distribution in Dye Sensitised Nanocrystalline Solar Cells by Intensity Modulated Photocurrent Spectroscopy (IMPS). *Electrochem. Commun.* **1999**, *1*, 61-64.
(38) Ponomarev, E. A.; Peter, L. M. A Generalized Theory of Intensity Modulated Photocurrent Spectroscopy (IMPS). *J. Electroanal. Chem.* **1995**, *396*, 219-226.
(39) Peter, L. M.; Ponomarev, E. A.; Fermín, D. J. Intensity-Modulated Photocurrent Spectroscopy: Reconciliation of Phenomenological Analysis with Multistep Electron Transfer Mechanisms. *J. Electroanal. Chem.* **1997**, *427*, 79-96.
(40) Peter, L. M.; Wijayantha, K. G. U.; Tahir, A. A. Kinetics of Light-Driven Oxygen Evolution at alpha-Fe2O3 Electrodes. *Farad. Discuss.* **2012**, *155*, 309-322.
(41) Grancini, G.; Marras, S.; Prato, M.; Giannini, C.; Quarti, C.; De Angelis, F.; De Bastiani, M.; Eperon, G. E.; Snaith, H. J.; Manna, L., et al. The Impact of the Crystallization Processes on the Structural and Optical Properties of Hybrid Perovskite Films for Photovoltaics. *J. Phys. Chem. Lett.* **2014**, *5*, 3836-3842.
(42) Gottesman, R.; Haltzi, E.; Gouda, L.; Tirosh, S.; Bouhadana, Y.; Zaban, A.; Mosconi, E.; De Angelis, F. Extremely Slow Photoconductivity Response of CH3NH3PbI3 Perovskites Suggesting Structural Changes under Working Conditions. *J. Phys. Chem. Lett.* **2014**, *5*, 2662–2669.
(43) Bertoluzzi, L.; Boix, P. P.; Mora-Sero, I.; Bisquert, J. Theory of Impedance Spectroscopy of Ambipolar Solar Cells with Trap-Mediated Recombination. *J. Phys. Chem. C* **2013**, *118*, 16574-16580.
(44) Brivio, F.; Walker, A. B.; Walsh, A. Structural and Electronic Properties of Hybrid Perovskites for High-Efficiency Thin-Film Photovoltaics from First-Principles. *APL Mat.* **2013**, *1*, 042111.
(45) Douglass Jr, E. F.; Driscoll, P. F.; Liu, D.; Burnham, N. A.; Lambert, C. R.; McGimpsey, W. G. Effect of Electrode Roughness on the Capacitive Behavior of Self-Assembled Monolayers. *Anal. Chem.* **2008**, *80*, 7670-7677.
(46) Im, J.-H.; Kim, H.-S.; Park, N.-G. Morphology-Photovoltaic Property Correlation in Perovskite Solar Cells: One-Step Versus Two-Step Deposition of CH3NH3PbI3. *APL Mat.* **2014**, *2*, 081510.
(47) Bass, K. K.; McAnally, R. E.; Zhou, S.; Djurovich, P. I.; Thompson, M. E.; Melot, B. C. Influence of Moisture on the Preparation, Crystal Structure, and Photophysical Properties of Organohalide Perovskites. *Chem. Commun.* **2014**, *50*, 15819-15822.
(48) Buin, A.; Pietsch, P.; Xu, J.; Voznyy, O.; Ip, A. H.; Comin, R.; Sargent, E. H. Materials Processing Routes to Trap-Free Halide Perovskites. *Nano Lett.* **2014**, *14*, 6281-6286.
(49) Guerrero, A.; Juarez-Perez, E. J.; Bisquert, J.; Mora-Sero, I.; Garcia-Belmonte, G. Electrical Field Profile and Doping in Planar Lead Halide Perovskite Solar Cells. *Appl. Phys. Lett.* **2014**, *105*, 133902.
(50) Peter, L. M. Dynamic Aspects of Semiconductor Photoelectrochemistry. *Chem. Rev.* **1990**, *90*, 753-769.

TOC figure:

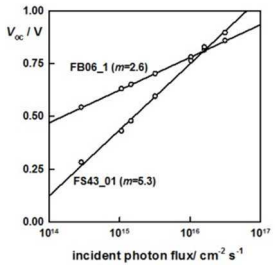
1.00
V_{oc} / V
0.75
0.50
0.25
0.00
FB06_1 (m=2.6)
FS43_01 (m=5.3)
10^{14}
10^{15}
10^{16}
10^{17}
incident photon flux/ cm^{-2} s^{-1}